The Astrophysical Journal Letters, 895:L10 (7pp), 2020 May 20 https://doi.org/10.3847/2041-8213/ab8e31

Observation of Energy Conversion Near the X-line in Asymmetric Guide-field Reconnection

J. Xu[1], F. Z. Peng[1,2], C. T. Russell[3], B. Giles[4], P.-A. Lindqvist[5], R. B. Torbert[6], R. E. Ergun[7], and J. L. Burch[8]
[1] School of Space and Environment, Beihang University, Beijing, People's Republic of China; fzpeng@buaa.edu.cn
[2] School of Physics, Beihang University, Beijing, People's Republic of China
[3] Institute of Geophysics and Planetary Physics, University of California, Los Angeles, CA, USA
[4] NASA Goddard Space Flight Center, Greenbelt, MD, USA
[5] Royal Institute of Technology, Stockholm, Sweden
[6] Physics Department and Space Science Center, University of New Hampshire, Durham, NH, USA
[7] Department of Astrophysical and Planetary Sciences, University of Colorado Boulder, Boulder, CO, USA
[8] Southwest Research Institute, San Antonio, TX, USA
Received 2019 November 10; revised 2020 April 24; accepted 2020 April 26; published 2020 May 19

Abstract

With high-resolution data of the recently launched Magnetospheric Multiscale mission, the present study reports an asymmetric guide-field reconnection at the dayside magnetopause, which has a density asymmetry $N_{\rm MSP}/N_{\rm MSH} \sim 15$ on the two sides of the current sheet and a guide field $B_g \sim 1.4B_{L,\ \rm MSH}$ in the out-of-plane direction, exhibiting all the two-fluid features including Alfvénic plasma jets and Hall field systems. Using the First Order Taylor Expansion method, we identify the X-line of this reconnection. Different from previous observations, the energy conversion dominantly occurs sunward of the X-line, while the local waves arise simultaneously. The qualitative analysis about the electron energization in this reconnection is proposed, suggesting that the guide field may play an important role in modifying the location where the energy conversion occurs together with the electric field near the X-line.

Unified Astronomy Thesaurus concepts: Magnetic fields (994); Plasma physics (2089); Planetary magnetosphere (997); Space plasmas (1544); Magnetohydrodynamics (1964)

1. Introduction

Magnetic reconnection is a fundamental plasma process responsible for the many explosive phenomena produced in space physics (Xiao et al. 2007; Retinò 2008; Cao et al. 2013; Fu et al. 2019). During the reconnection process, the field topology changes and simultaneously the energy stored in magnetic field is transferred to plasma particles (Øieroset et al. 2001; Mozer et al. 2002; Lavraud et al. 2016; Shay et al. 2016; Burch et al. 2018). The reconnection site of the X-line, where the field reaches the minimum in the reconnection plane, has been regarded as the location where energy conversion occurs, as it is coincident with the flow stagnation point during symmetric reconnection. However, reconnection at Earth's magnetopause is typically asymmetric, since the plasma density and magnetic field change significantly between the magnetosphere and magnetosheath side. The density asymmetry thus alters the momentum balance equation nearby the electron diffusion region (EDR), meaning the electron flow stagnation point is no longer collocated with the X-line but is shifted toward the low-density magnetospheric side (Cassak & Shay 2007; Pritchett & Mozer 2009; Norgren et al. 2016; Cassak et al. 2017). Asymmetric reconnection observations with a weak or null guide field have shown that the energy conversion between the field and electrons always occurs earthward of the X-line (Burch et al. 2016; Hwang et al. 2017). Comparing several cases of observed EDR events, Genestreti et al. (2017) demonstrated that the emergence of the guide field may play an important role in changing the location of energy conversion ($J \cdot E'$ region) during asymmetric reconnection. Simulations have shown that for asymmetric reconnection with weak guide fields, the energy conversion occurs at the magnetospheric side (earthward) of the X-line, midway between the X-line and electron stagnation point, and moves toward the electron stagnation point with an increasing guide field (Cassak et al. 2017).

It is still a puzzle to determine how the energy conversion is motivated and where such energy conversion occurs with the effects of guide field, owing to the absence of high-resolution satellite observation (Hoshino 2012; Walsh et al. 2012; Genestreti et al. 2017). In this Letter, we report an asymmetric guide-field magnetic reconnection on 2015 December 3 at Earth's magnetopause. With the First Order Taylor Expansion (FOTE) method, which was developed recently to recognize the magnetic nulls (Fu et al. 2015), we identify the X-line around the reversal time in this reconnection. The energy conversion between field and electrons occurring sunward of the X-line is found here, which is clearly different from previous observations. The positive $\boldsymbol{Je} \cdot \boldsymbol{E}$ (electron dissipation) is mainly distributed in the out-of-plane direction, indicating that the guide field could modify the location of the energy conversion together with the electric field nearby the EDR during magnetic reconnection. These results could be important for future simulations and observations studying the energization mechanisms in asymmetric guide-field reconnection.

2. Data and Instrumentation

The data from MMS mission (Burch et al. 2015), particularly from the Fluxgate Magnetometers, Electric Double Probe, and the Fast Plasma Instruments on board it, are used in this Letter (Lindqvist et al. 2016; Pollock et al. 2016; Russell et al. 2016; Torbert et al. 2016). The local current sheet coordinate system (LMN) is also presented here. With respect to the geocentric

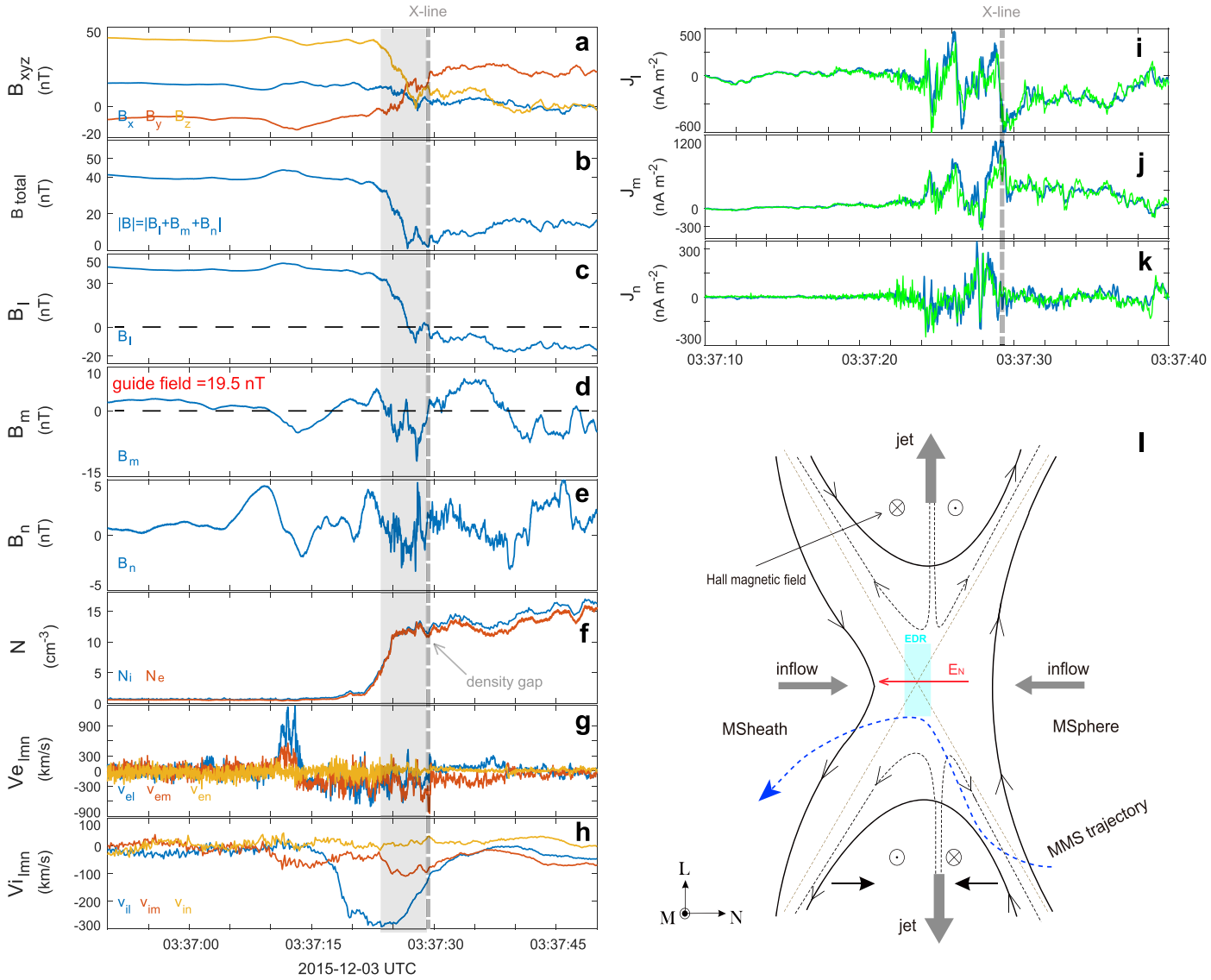

Figure 1. Overview of the reconnection event on 2015 December 3. (a) The three components of the magnetic field in GSE coordinates. (b) The total magnetic field with a guide field of 19.5 nT is subtracted. (c)–(e) Magnetic field B_L, B_M, and B_N components in LMN coordinates. (f) The number density of ions and electrons. (g)–(h) The electron and ion flow velocity. (i)–(k) The three components of the current density in LMN coordinates, with the green line calculated from plasma moments, while the blue line is computed from $\nabla \times \boldsymbol{B}$. (l) A cartoon showing the asymmetric Hall reconnection at the magnetopause. In panel (d), the guide field $B_g = 19.5$ nT has been subtracted.

solar ecliptic (GSE) coordinates, $\boldsymbol{L} = [0.24, -0.62, 0.75]$, $\boldsymbol{M} = [0.25, 0.78, 0.57]$, and $\boldsymbol{N} = [-0.94, 0.05, 0.34]$.

3. Observations

The reconnection of interest was observed on 2015 December 3 around 03:37:25 UT, when the four MMS spacecraft were at the magnetopause with a separation of ~10 km ([11.3, −1.8, −0.8] R_E in GSE coordinates). Such a small separation makes all four spacecraft generally measure similar field and plasma properties. For the purpose of simplicity, we show only data from MMS1 in this study.

Figure 1 shows the overview of this event from 03:37:00 to 03:37:50 UT. As can be seen, the magnetic field changes dramatically at ~03:37:30 UT (Figure 1(a)), and the field magnitude $B_{\rm total}$ reaches its minimum at 03:37:29 UT (Figure 1(b)). Also, the magnetic field in the L direction B_L changes from positive (northward, +40 nT) to negative (southward, −15 nT) at ~03:37:29 UT, indicating the encounter of a current sheet at this time (Figure 1(c), see the vertical dashed line). From Figure 1(d), we find that the field in the M direction B_m has a bipolar signature around the B_L reversal time of 03:37:29 UT, which changes from −13 to +8 nT. It should be noted that the guide field B_g of ~+19.5 nT that was calculated from the average value of B_m during the whole interval has been subtracted here. This bipolar signature represents the quadrupolar Hall magnetic fields in reconnection. The plasma density ratio between the magnetosphere and magnetosheath sides almost reaches 15 in this event (see Figure 1(f)). A density dip has been found at 03:37:29 UT where the magnetic field B_L reversed, and this reversal time then will be identified to the X-line encounter with the FOTE method. As presented in Figure 1(h), the southward ion flow reaches its peak of 300 km s^{-1} at ~03:37:23.5 UT. This jet velocity is comparable to the upstream Alfvén speed $V_A = \sqrt{\frac{B_1 B_2 (B_1 + B_2)}{\mu_0(\rho_1 B_1 + \rho_2 B_2)}}$ ~266 km s^{-1} ($\rho_1 = N_1$mi, $\rho_2 = N_2$mi),

where $B_1 \approx 40$ nT, $B_2 \approx 15$ nT and $N_1 \approx 1\,\mathrm{cm}^{-3}$, $N_2 \approx 15\,\mathrm{cm}^{-3}$ are respectively the reconnecting field and number density on the two sides of current sheet (Cassak & Shay 2007). The current densities J_L, J_M, and J_N in LMN coordinates are shown in Figures 1(i)–(k), where the blue line denotes the current density calculated from the curlometer method, while the green line represents the current density derived from the moment formula of $J = \boldsymbol{n} \cdot \boldsymbol{e} \cdot (\boldsymbol{V}_i - \boldsymbol{V}_e)$. As clearly shown, the current densities derived from these two methods are quite similar due to the high-resolution data provided by MMS satellites. The current in the L direction J_L presents the Hall current variation during 03:37:24–03:37:38 UT, which is consistent with the bipolar signature of Hall fields (see Figures 1(d), (i) and the cartoon in Figure 1(l)). Also, the intense current in the M direction J_M mainly occurs at around 03:37:29 UT, corresponding to the current sheet in the out-of-plane direction. All of these observations correspond well to the reconnection crossing shown in Figure 1(l) (the MMS trajectory is marked in blue), where we interpreted the spacecraft crossed southward of this guide-field reconnection from the magnetosphere to magnetosheath side.

4. Magnetic Field Topology

After the removal of the guide field (Figure 1(d)), we were able to examine the magnetic nulls inside the current sheet of this reconnection. We used the FOTE method (Fu et al. 2015) to calculate the distance between magnetic nulls and spacecraft, and we also identified the null types in this event. The results are shown in Figures 2(a)–(e), including (a) the magnetic field in the L direction of the four MMS satellites, (b) the distance from magnetic null to each of the four spacecraft, i.e., the null-SC distance $|r|$, (c) the minimum null-SC distance with null types labeled, and (d)–(e) the two parameters, $\eta \equiv |\nabla \cdot B|/|\nabla \times B|$ and $\xi \equiv |\lambda 1 + \lambda 2 + \lambda 3|/|\lambda|\,\mathrm{max}$, for quantifying the quality of the FOTE results. Here λ_1, λ_2, and λ_3 are the three eigenvalues of the Jacobian matrix $\nabla \boldsymbol{B}$ that can be constructed using four-spacecraft measurements, and $|\lambda|_{\mathrm{max}}$ is the maximum of the norm of these three eigenvalues. According to the relationship among these eigenvalues, the magnetic null can be categorized into different types, as shown in Figure 2(c) (see Section 2.3 in Fu et al. 2015 for details).

During the crossing of current sheet (03:37:28.6–03:37:29.4 UT), we find magnetic nulls with null-SC distances smaller than 60 km (Figure 2(b)), i.e., nearly the local ion inertial length $d_{\mathrm{i}} = c/\omega_{\mathrm{pi}}$ (58 km, with a local ion number density of $13\,\mathrm{cm}^{-3}$). In this event, the magnetic null of the "X-line" closest to the spacecraft is found at 03:37:29.23 UT within the limitation of best method quality (Figure 2(c), see the dashed line), coinciding with the B_L reversal time of MMS1 (Figure 1(c)). The identification of this X-line should be very reliable, because (1) the null-SC distance is only about 7 km (which is about 0.1 ion inertial length or 3.6 electron inertial lengths; see Figure 2(c)) and (2) the parameters η and ξ are also small ($\eta < 3\%$ and $\xi < 3\%$; see Figures 2(d)–(e)). We therefore reconstruct the magnetic topology of this null and show it in Figures 2(f) and (g). As can be seen, the magnetic field topology around satellites within 60 km clearly shows the X-line structure, consistent with the theoretical prediction of the topology of the X-line after the removal of the guide field. Here the topology is obtained by tracing the magnetic fields around the spacecraft tetrahedron (see Fu et al. 2015 for details). Although the X-line result got here does not mean the real magnetic null of this reconnection (because the guide field exists through the whole crossing), this result still indicates the X-line or EDR is nearby in the reconnection plane.

5. Electron Distributions and the $Je \bullet E$ Region Near the X-line

Figures 3(a)–(b) present the pitch angle distributions of electrons within the middle (0.2–2 keV) and high (2–30 keV) energy in detail around the X-line. Shown in Figure 3(b), the energetic electrons (with a high energy much larger than the local electron thermal temperature of ~65 eV) exhibit a clear pitch angle of 0° and 180° from 03:37:26 UT to 03:37:32 UT. These field-lined energetic particles might be the electrons accelerated at the reconnection separatrix of the magnetosphere and magnetosheath sides, which flow along the reconnected field lines and toward the X-line showing such parallel and antiparallel distributions. It should be noted that the energetic electrons also presented the antiparallel distributions at the X-line, where the magnetic field lines "broke" and "reconnected" (see the dashed line marked in gray; 03:37:29.23 UT). These antiparallel populations at the X-line should be the electrons transported along the reconnected field from magnetosheath to magnetosphere, which were driven by the density pressure of the two sides (see Figure 1(f)).

The electron energy conversion ($\boldsymbol{Je} \cdot \boldsymbol{E}$) during the whole crossing is shown in Figure 3(c). To investigate the energy conversion around the X-line recognized at 03:37:29.23 UT, the detailed views of the electron velocity, the electric field, and the dissipation quantity of $\boldsymbol{Je} \cdot \boldsymbol{E}$ are plotted in Figures 3(d)–(i) from 03:37:29 to 03:37:30 UT. As shown in the comparison between the electric field and convection term (Figures 3(e)–(g)), the frozen-in condition of particles is dramatically broken during the whole interval ($E \neq -\boldsymbol{V}_i \times \boldsymbol{B}$; $E \neq -\boldsymbol{V}_e \times \boldsymbol{B}$), indicating ions and electrons are indeed demagnetized or the particle energy is dissipated. Figure 3(h) shows that the average value of $\boldsymbol{Je} \cdot \boldsymbol{E}$ during this dissipation region from 03:37:29.23–03:37:29.90 UT is positive, meaning that the energy of the magnetic field was transported to electrons. Different from previous observations, we find that the electric field system and energy conversion mainly occur sunward of the X-line (see the vertical dashed line), instead of at the region between the X-line and electron flow stagnation point, namely, earthward of the X-line (low-density side of the current sheet). Genestreti et al. (2018) have also reported recently a similar magnetopause reconnection with energy conversion observed on the magnetosheath side near the X-line.

This energy conversion between field and electrons could be interpreted as the effects caused by the guide field and wave–particle interactions. In the reconnection plane, the electrons near the X-line could be magnetized by the large guide field along the out-of-plane direction. As shown in Figure 3(d), the electron flow along the negative M direction actually shows such magnetization. Also, the electric field in the N direction E_N increased to about 10 mV m^{-1} around 03:27:29.6 UT, which will be illustrated to be likely generated by the local waves. Therefore, the electrons will then be affected by the force of $E_N \times B_g$ and drift along the L direction. These electrons along the $-M$ and $+L$ directions thus could be accelerated by positive E_M and negative E_L, or decelerated by negative E_M and positive E_L. As shown in Figures 3(e)–(f) and (i), the positive E_M indeed correspond to the positive $\boldsymbol{Je} \cdot \boldsymbol{E}$ in the M direction; the positive E_L and negative E_L are

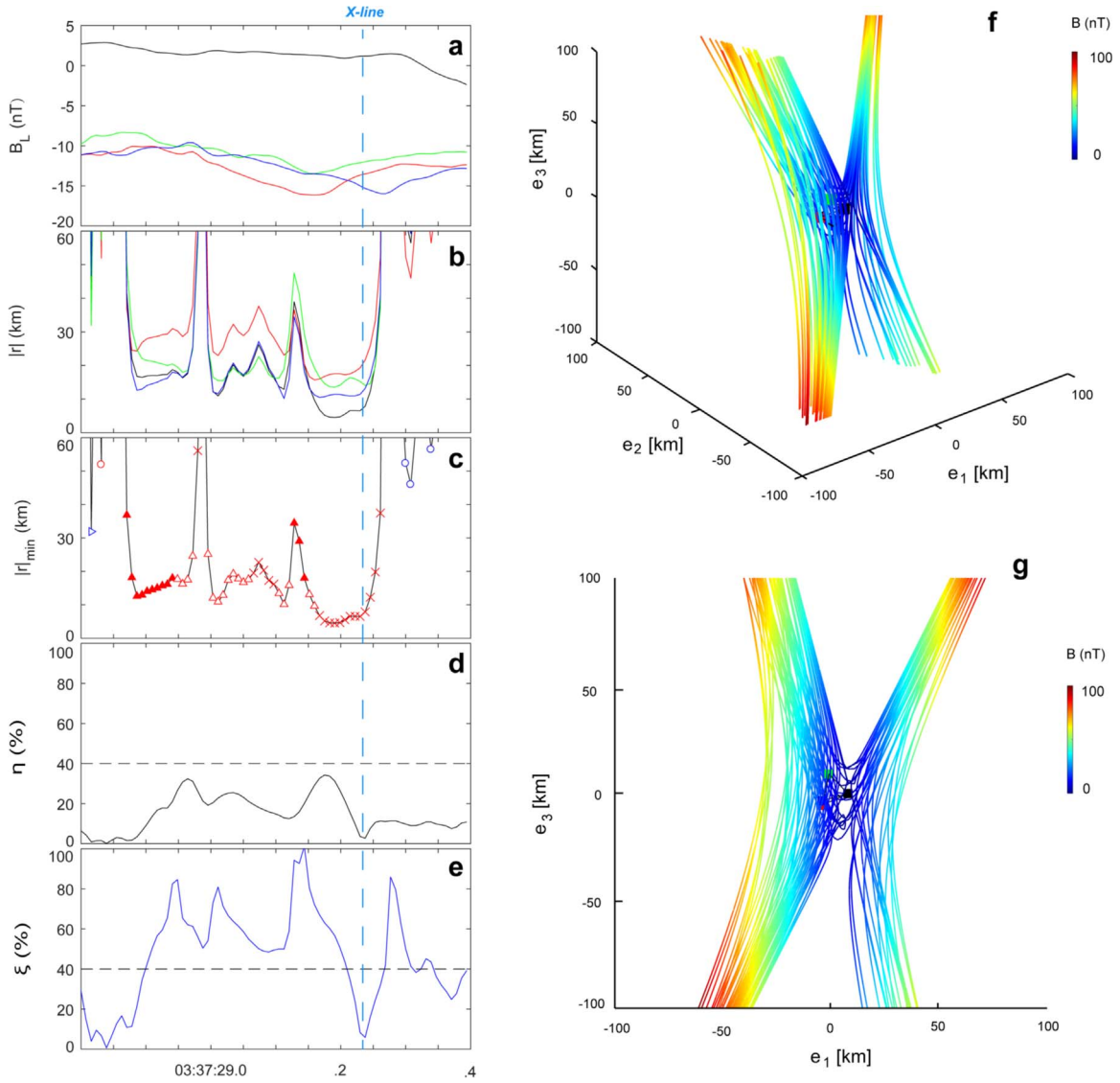

Figure 2. FOTE analysis of the magnetic reconnection event on 2015 December 3. (a) Magnetic field in the L direction of $B_{\rm L}$ from 03:37:28.6 to 03:37:30.4 UT. (b) Distance from magnetic null to each of the four spacecraft, i.e., the null-SC distance. (c) The minimum null-SC distance with null types labeled. (d)–(e) The two parameters, η and ξ, for quantifying the quality of the FOTE results. (f)–(g) The topology constructed around the magnetic null at 03:37:29.23 UT. The eigenvector coordinate system $\boldsymbol{e}_1$ $\boldsymbol{e}_2$ $\boldsymbol{e}_3$ is used in Figures 2(f) and (g). With respect to the original GSE coordinates, $\boldsymbol{e}_1 = [-0.41\ -0.37\ -0.83]$, $\boldsymbol{e}_2 = [0.67\ -0.74\ 0]$, and $\boldsymbol{e}_3 = [-0.61\ -0.56\ 0.56]$.

respectively consistent with the negative and positive $\boldsymbol{Je} \cdot \boldsymbol{E}$ in the L direction. All of the above observations verify that the guide field plays an important role in modifying the location where the energy conversion occurs during asymmetric reconnection, together with the electric field near the EDR.

To examine the emergence of local electric fields, we investigated the wave emissions nearby the X-line in Figure 4. We found that during the enhancement of energy conversion (03:27:29.3–03:27:29.9 UT), strong wave emissions also appeared with frequencies of below the low hybrid frequency of $f_{\rm lh}$, above the electron cyclotron frequency of $f_{\rm ce}$, and between $f_{\rm lh}$ and $0.1f_{\rm ce}$ (Figures 4(c)–(g)). Different from the emissions above $f_{\rm ce}$ and below $f_{\rm lh}$, the waves with frequencies between $f_{\rm lh}$ and $0.1f_{\rm ce}$ show the clear propagation angle of $\sim 0^\circ$–20° and simultaneously owned the good planarity and negative ellipticity (see Figures 4(j)–(l)), which might contribute to the local wave–particle interactions. As shown in Figures 4(b)–(c), the electric field oscillations of waves between $f_{\rm lh}$ and $0.1f_{\rm ce}$ correspond well to the electric field system, indicating the local electric field might be generated by these local waves (Liu et al. 2009). Since the ambient magnetic field is nearly the same as $\boldsymbol{B}_{\rm M}$ (see Figure 4(a)), the quasi-parallel propagation property of the waves between $f_{\rm lh}$ and $0.1f_{\rm ce}$ (see Figure 4(k)) illustrates these waves propagate out of the plane, suggesting the local increasing electric fields might be attributed to these local waves beyond the 2D picture. Also, the field-aligned Poynting fluxes of waves between $f_{\rm lh}$ and $0.1f_{\rm ce}$ change the sign at 03:27:29.46 UT (see Figure 4(m)), indicating that the spacecraft may pass the source region of the waves, which shows a nice correlation with the energy conversion region.

6. Discussions and Conclusions

We present a case study of asymmetric magnetic reconnection at Earth's magnetopause on 2015 December 3, where the large guide field of $\sim$20 nT nearly approaches the equivalent of the reconnection field on the magnetosheath side. The plasma

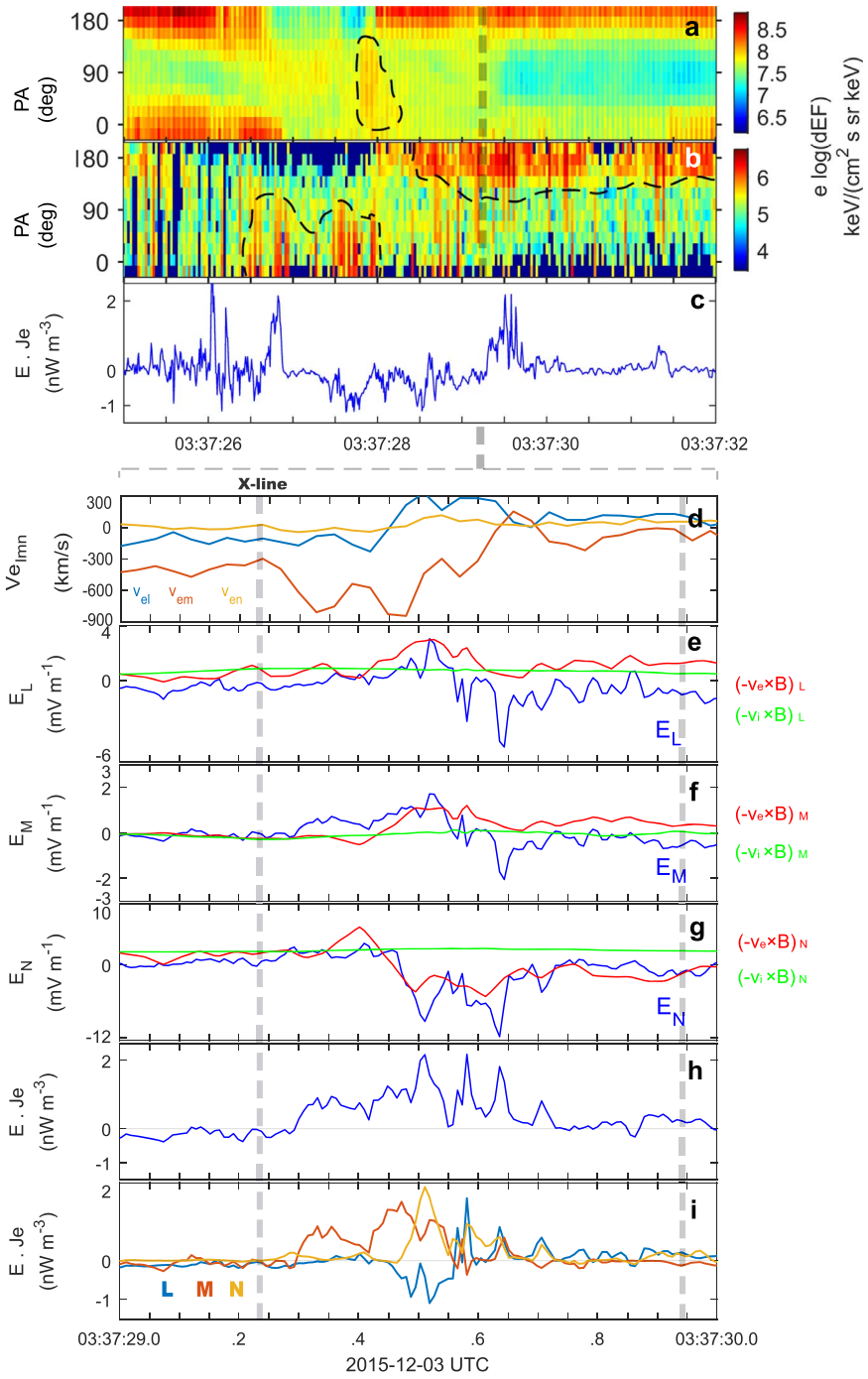

Figure 3. (a)–(b) The pitch angle distributions of middle (0.2–2 keV) and high (2–30 keV) energy electrons observed from 03:37:25 to 03:37:32 UT. (c) The energy conversion term of $\boldsymbol{Je} \cdot \boldsymbol{E}$ during 03:37:25–03:37:32 UT. (d) A close-up view of the electron velocity in the L, M, and N directions during 03:37:29–03:37:30 UT. (e)–(g) A close-up view of the electric field in the L, M, and N directions during 03:37:29–03:37:30 UT, where the electron convection term $-\boldsymbol{V}_e \times \boldsymbol{B}$ is represented in red and the ion convection term $-\boldsymbol{V}_i \times \boldsymbol{B}$ is shown in green. (h) The total dissipation term of $\boldsymbol{Je} \cdot \boldsymbol{E}$. (i) The dissipation term of $\boldsymbol{Je} \cdot \boldsymbol{E}$ in the three components of the L, M, and N directions.

density discrepancy on the magnetosphere and magnetosheath sides of the current sheet is about ∼15 ($N_{\rm pla.MSH}/N_{\rm pla.MP}$), which is strong enough to distort the Hall magnetic field region as in traditional simulation results (e.g., Rogers et al. 2003; Huba 2005; Tanaka et al. 2008; Pritchett & Mozer 2009; Eastwood et al. 2010, 2013; Zhang et al. 2017). However, the quadrupolar pattern of Hall fields were still shown during this guide-field asymmetric reconnection, verifying the interpretation of quadrupolar Hall fields in Peng et al. (2017).

With the MMS data and FOTE method, we recognized the X-line around the reversal time in this asymmetric guide-field reconnection. The energy conversion is found to locate sunward of the X-line, which shows a different picture from previous observations. The local wave–particle interactions and the effect caused by the guide field are discussed to interpret this observation of energy conversion. During the crossing of the current sheet, the magnetic fields in the L and N directions are both near to zero, thus only the field in the M direction of

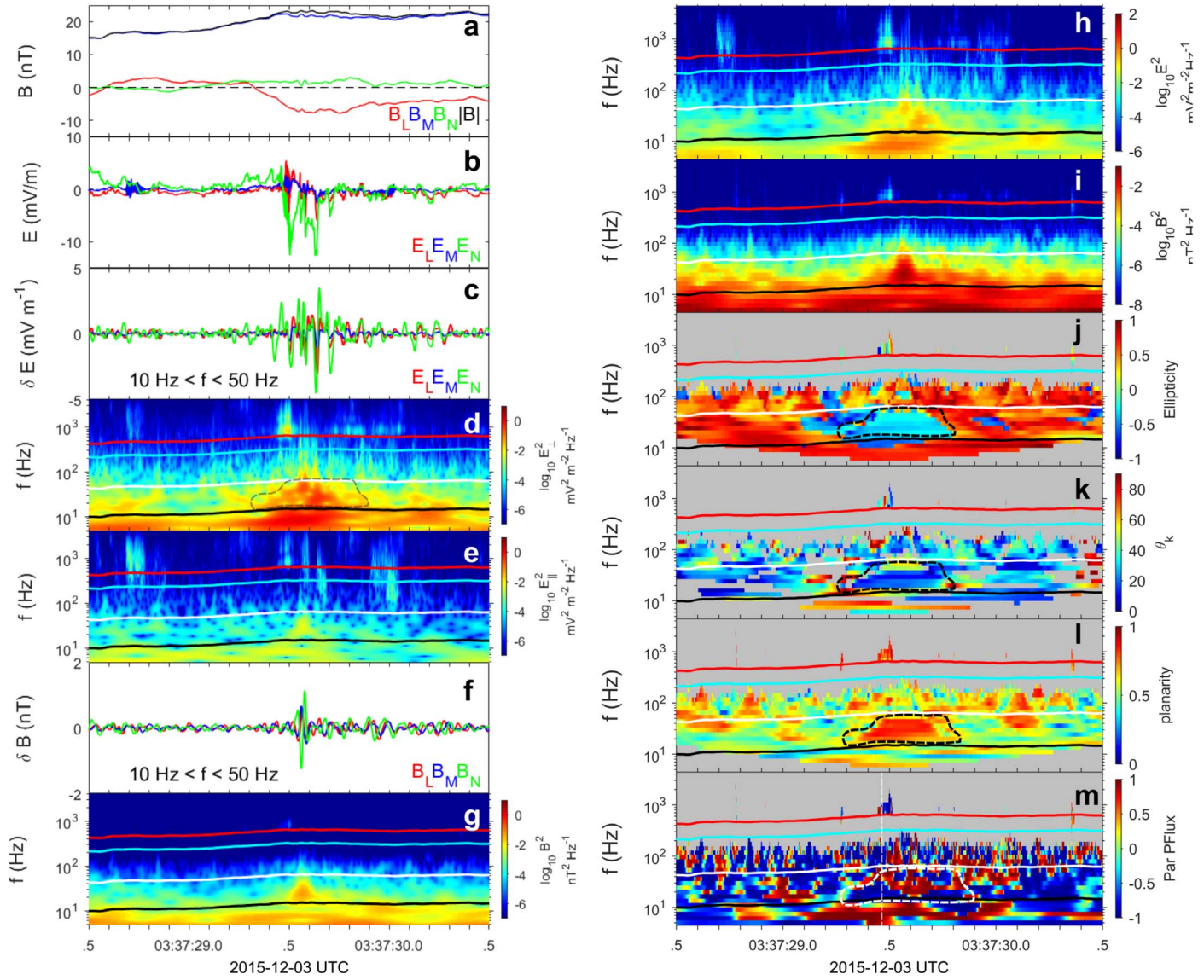

Figure 4. Plasma properties and magnetic fields during 03:37:28.5–03:37:30.5 UT (left column), including (a) the magnetic field systems; (b) the electric field systems; (c) the filtered electric field between 10 Hz and 50 Hz in LMN coordinates; (d)–(e) the electric field power spectrogram; (f) the filtered magnetic field between 10 Hz and 50 Hz in LMN coordinates; (g) the magnetic field power spectrogram and wave polarization analysis (right column), including (h)–(i) power spectra density of the electric and magnetic field components of waves; (j) the ellipticity of the waves, with +1 denoting the right-handed circular polarization and −1 denoting the left-handed circular polarization; (k) the wave normal angle; (l) the wave planarity; and (m) the parallel Poynting flux (positive values indicate propagation parallel to the magnetic field and negative values indicate propagation antiparallel to the magnetic field). The colored lines in Figures 4(d)–(e) and (g)–(m) denote f_{ce} (red), $0.5f_{ce}$ (cyan), $0.1f_{ce}$ (white), and f_{lh} (black). Here f_{ce} is the local electron cyclotron frequency and f_{lh} is the low hybrid frequency.

$\boldsymbol{B}_M$ could trap the electrons near the X-line. However, the guide field of $\sim$+19.5 nT was neutralized by the negative Hall field of ~-13 nT on the magnetosphere side, namely, earthward of the X-line, which might be too weak to trap the electrons. Therefore, the electrons could be mainly magnetized by the large magnetic field along the M direction caused by the positive Hall field and guide field $\boldsymbol{B}_g$ sunward of the X-line. We clearly showed how the magnetized electrons along the guide field could be drifted by the force of $E_N \times B_g$ and accelerated by the different electric field systems, which might be generated by the local waves with frequencies between f_{lh} and f_{ce}. All of the observations are well consistent with each other. The results imply that the guide field can modify the location of the energy conversion together with the electric field nearby the X-line. The present study shown here is important to understand the energy conversion during reconnection, and more high-resolution MMS data could be used in the future to study the energy conversion in asymmetric guide-field reconnection.

We thank the MMS Science Data Center (https://lasp.colorado.edu/mms/sdc/public/) for providing the data for this study. This work is supported by the National Natural Science Foundation of China under grants No. 41231066, No. 41574154, No. 11522539, and No. 11735003.

ORCID iDs

J. Xu https://orcid.org/0000-0003-2375-8693
F. Z. Peng https://orcid.org/0000-0003-1292-5943
C. T. Russell https://orcid.org/0000-0003-1639-8298
B. Giles https://orcid.org/0000-0001-8054-825X
P.-A. Lindqvist https://orcid.org/0000-0001-5617-9765
R. B. Torbert https://orcid.org/0000-0001-7188-8690

R. E. Ergun https://orcid.org/0000-0002-3096-8579
J. L. Burch https://orcid.org/0000-0003-0452-8403

References

Burch, J. L., Ergun, R. E., Cassak, P. A., et al. 2018, GeoRL, 45, 1237
Burch, J. L., Moore, T. E., Torbert, R. B., & Giles, B. L. 2015, SSRv, 199, 5
Burch, J. L., Torbert, R. B., Phan, T. D., et al. 2016, Sci, 352, aaf2939
Cao, J. B., Wei, X. H., Duan, A. Y., et al. 2013, JGRA, 118, 1659
Cassak, P. A., Genestreti, K. J., Burch, J. L., et al. 2017, JGRA, 122, 11523
Cassak, P. A., & Shay, M. A. 2007, PhPl, 14, 102114
Eastwood, J. P., Phan, T. D., Oieroset, M., et al. 2013, PlPh, 55, 124001
Eastwood, J. P., Shay, M. A., Phan, T. D., & Øieroset, M. 2010, PhRvL, 104, 205501
Fu, H. S., Peng, F. Z., Liu, C. M., et al. 2019, GeoRL, 46, 5645
Fu, H. S., Vaivads, A., Khotyaintsev, Y. V., et al. 2015, JGRA, 120, 3758
Genestreti, K. J., Burch, J. L., Cassak, P. A., et al. 2017, JGRA, 122, 11342
Genestreti, K. J., Varsani, A., Burch, J. L., et al. 2018, JGRA, 123, 1806
Hoshino, M. 2012, PhRvL, 108, 135003
Huba, J. D. 2005, PhPl, 12, 322
Hwang, K. J., Sibeck, D. G., Choi, E., et al. 2017, GeoRL, 44, 2049
Liu, W., Sarris, T. E., Li, X., et al. 2009, JGRA, 114, A12206
Lavraud, B., Zhang, Y. C., Vernisse, Y., et al. 2016, GeoRL, 43, 3042
Lindqvist, P. A., Olsson, G., Torbert, R. B., et al. 2016, SSRv, 199, 137
Mozer, F. S., Bale, S. D., & Phan, T. D. 2002, PhRvL, 89, 15002
Norgren, C., Graham, D. B., Khotyaintsev, Y. V., et al. 2016, GeoRL, 43, 6724
Øieroset, M., Phan, T., Fujimoto, M., Lin, R., & Lepping, R. 2001, Natur, 412, 414
Peng, F. Z., Fu, H. S., Cao, J. B., et al. 2017, JGRA, 122, 6349
Pollock, C., Moore, T., Jacques, A., et al. 2016, SSRv, 199, 331
Pritchett, P. L., & Mozer, F. S. 2009, JGRA, 114, A11210
Retinò, A., Nakamura, R., Vaivads, A., et al. 2008, JGRA, 113, A12215
Rogers, B. N., Denton, R. E., & Drake, J. F. 2003, JGRA, 108, 1111
Russell, C. T., Anderson, B. J., Baumjohann, W., et al. 2016, SSRv, 199, 189
Shay, M. A., Phan, T. D., Haggerty, C. C., et al. 2016, GeoRL, 43, 4145
Tanaka, K. G., Retinò, A., Asano, Y., et al. 2008, AnGeo, 26, 2471
Torbert, R. B., Russell, C. T., Magnes, W., et al. 2016, SSRv, 199, 105
Walsh, B. M., Haaland, S. E., Daly, P. W., Kronberg, E. A., & Fritz, T. A. 2012, AnGeo, 30, 1003
Xiao, C. J., Pu, Z. Y., Wang, X. G., et al. 2007, GeoRL, 34, L01101
Zhang, Y. C., Lavraud, B., Dai, L., et al. 2017, JGRA, 122, 5277